Cell, Vol. 97, 657–666, May 28, 1999, Copyright ©1999 by Cell Press

# Crystal Structure of a Phosphatidylinositol 3-Phosphate-Specific Membrane-Targeting Motif, the FYVE Domain of Vps27p

**Saurav Misra and James H. Hurley***
Laboratory of Molecular Biology
National Institute of Digestive, Diabetes, and Kidney Diseases
National Institutes of Health
Bethesda, Maryland 20892-0580

## Summary

**Phosphatidylinositol 3-phosphate regulates membrane trafficking and signaling pathways by interacting with the FYVE domains of target proteins. The 1.15 Å structure of the Vps27p FYVE domain reveals two antiparallel β sheets and an α helix stabilized by two $Zn^{2+}$-binding clusters. The core secondary structures are similar to a rabphilin-3A $Zn^{2+}$-binding domain and to the C1 and LIM domains. Phosphatidylinositol 3-phosphate binds to a pocket formed by the (R/K)(R/K)HHCR motif. A lattice contact shows how anionic ligands can interact with the phosphatidylinositol 3-phosphate-binding site. The tip of the FYVE domain has basic and hydrophobic surfaces positioned so that nonspecific interactions with the phospholipid bilayer can abet specific binding to phosphatidylinositol 3-phosphate.**

## Introduction

Signal transduction through D3-phosphorylated phosphoinositides is the subject of intensive investigation because these lipids play key roles in receptor signaling at the plasma membrane (Toker and Cantley, 1997; Corvera and Czech, 1998; Fruman et al., 1998) and in membrane trafficking within the cell (De Camilli et al., 1996; Corvera and Czech, 1998). Phosphatidylinositol (3,4) bisphosphate [$PI(3,4)P_2$] and phosphatidylinositol (3,4,5) trisphosphate ($PIP_3$) are the principal products of class I and II phosphoinositide 3-kinases (PI3Ks). $PI(3,4)P_2$ can also be produced by the type II phosphatidylinositol phosphate kinases (PIPKs) (Fruman et al., 1998). These phosphoinositides are best known for their roles in receptor signaling at the plasma membrane (Toker and Cantley, 1997; Corvera and Czech, 1998; Irvine, 1998). Phosphatidylinositol 3-phosphate (PI3P) is the product of Vps34p and related class III PI3Ks (Fruman et al., 1998). It has recently become clear that PI3P is a pivotal regulator of membrane trafficking in yeast and animal cells (De Camilli et al., 1996). PI3P also has roles to play in signal transduction, for example via the TGF-β receptor (Tsukazaki et al., 1998), and in insulin regulation of adipocytes (Shisheva et al., 1999).

A decade-long search for the direct targets of signaling through 3-phosphorylated phosphoinositides culminated in the past two years with the identification of two structural classes of receptor. The bis- and trisphosphorylated phosphoinositides, $PI(3,4)P_2$ and $PIP_3$, activate their best known targets, including the kinases PDK1 and PKB, by binding to a subgroup of pleckstrin homology (PH) domains specific for these lipids (reviewed by Corvera and Czech, 1998; Irvine, 1998). The principal cellular receptors for the singly phosphorylated PI, PI3P, with a few exceptions do not have PH domains. Instead, these receptors have in common a conserved ~70 amino acid region known as a FYVE domain (Stenmark et al., 1996; Wurmser et al., 1999). Specific binding of PI3P by FYVE domains has recently been directly demonstrated in simultaneous reports from three different groups (Burd and Emr, 1998; Gaullier et al., 1998; Patki et al., 1998). One of the best characterized FYVE domain–containing proteins is the Rab5 effector EEA1, a core component of the endosome-docking apparatus (Mu et al., 1995; Patki et al., 1997; Simonsen et al., 1998; Christoforidis et al., 1999). The FYVE domain of EEA1 is essential for its correct targeting and endocytic function in cells (Burd and Emr, 1998), as shown by mutagenesis of the conserved (R/K)(R/K)HHCR motif. Indeed, all of the known direct effects of PI3P are mediated by FYVE domains.

We initiated attempts to crystallize the extended variant of the FYVE domain of EEA1 described by Burd and Emr (1998). When this was unsuccessful, we focused on the minimal FYVE domains of EEA1, Fab1p, and Vps27p. The latter two proteins are products of yeast genes required for protein sorting (Piper et al., 1995; Odorizzi et al., 1998). Fab1p is a PI3P 5-kinase that regulates membrane homeostasis (Gary et al., 1998; Odorizzi et al., 1998). Vps27p is the putative yeast counterpart of the mammalian protein Hrs and is involved in endosome maturation (Wurmser et al., 1999). Crystals were obtained immediately with the Vps27p FYVE domain, and we report the structure here refined at 1.15 Å resolution.

## Results

### Structure of the FYVE Domain

The FYVE domain of Vps27p, consisting of residues 169–229, was isolated as a monomer as judged by gel filtration (data not shown) and crystallized with one molecule per asymmetric unit. The structure was determined by multiwavelength anomalous dispersion (MAD; Hendrickson, 1991) at the Zn K edge using scattering from two native $Zn^{2+}$ ions (Table 1). The density-modified MAD phased map at 3.2 Å resolution revealed the entire polypeptide chain with no breaks and revealed all side chains (Figure 1A). The initial model was refined against all native data to 1.15 Å (Table 2; Figure 1B), with 5% of the data removed for cross-validation (Brünger, 1992). The solved structure includes six C-terminal residues (EFIVTD) derived from the expression vector, designated V1–V6. The current working R factor is 0.174, and the free R factor is 0.181 for all measured reflections to 1.15 Å resolution.

The FYVE domain structure consists of long loops at

*To whom correspondence should be addressed (e-mail: jh8e@nih.gov).

Table 1. Crystallographic Data and Phasing

| | | | | | |
|---|---|---|---|---|---|
| Space group | P1 | | | | |
| Cell dimensions | a = 24.1 Å, b = 26.5 Å, c = 31.8 Å, α = 112.0°, β = 92.5°, γ = 105.7° | | | | |
| | $d_{min}$ (Å) | No. of Reflections | Completeness | <I>/<σ> | $R_{sym}$[a] (%) |
| Zinc $\lambda_1$ (1.2830 Å)[b] | 2.0 | 4,494 (395)[c] | 95.4 (82.3) | 18.6 (8.0) | 6.5 (11.0) |
| Native (0.9797 Å) | 1.15 | 23,055 (2,188) | 94.0 (89.9) | 17.0 (3.4) | 6.3 (32.9) |

Observed Dispersive and Bijvoet Ratios[d]

| | $\lambda_1$ | $\lambda_2$ | $\lambda_3$ |
|---|---|---|---|
| $\lambda_1$ | 0.062 | 0.014 | 0.043 |
| $\lambda_2$ | | 0.062 | 0.035 |
| $\lambda_3$ | | | 0.053 |
| Figure of merit | | 0.85 (0.87) | |

[a] $R_{sym} = \Sigma_h\Sigma_i||I_i(h) - <I(h)>|/\Sigma_h\Sigma_i I_i(h)$.
[b] Statistics for $\lambda_2$ (1.2822 Å), $\lambda_3$ (1.2320 Å) were very similar to those for $\lambda_1$.
[c] Values in parentheses are for the highest-resolution bin.
[d] Ratios are calculated as $<\Delta|F|>/<|F|>$, using data between 5 and 2.5 Å.

the N terminus and between 209–218, two $Zn^{2+}$-binding clusters, two double-stranded antiparallel β sheets, and a C-terminal α helix (Figures 1C and 1D). β1 and β2 form the first sheet and β3 and β4 the second. Four residues of the N-terminal loop approximate an additional β strand in the first β sheet. Residues 170–173 are all in a β conformation but are not classified as a β strand because they do not conform to the standard β sheet hydrogen bonding pattern. The only such hydrogen bond is formed by the main chain at 171. It makes a β sheet hydrogen bond to residue 196, immediately preceding strand β2. After residue 171, this section pulls away from the first β sheet. The normal hydrogen bonds to the main chain are replaced by the side chains of His-191 (Nε to 171 O), Asp-172 (Oδ to 173 N), and Lys-189 (Nζ to 173 O). Residues 209–218 form a loop that swings away from the rest of the protein. The loop is separated from the C-terminal helix by an ~7 Å wide water-filled groove and from the first Zn cluster by another water-filled groove.

The structure is stabilized by two $Zn^{2+}$-binding clusters and by a small hydrophobic core. A chain of buried and partially buried hydrophobic residues runs through the center of the protein. From one side to the other, the chain consists of Phe-183, Val-198, Phe-199, Val-221, Ile-208, and Leu-210. The first $Zn^{2+}$ cluster contains

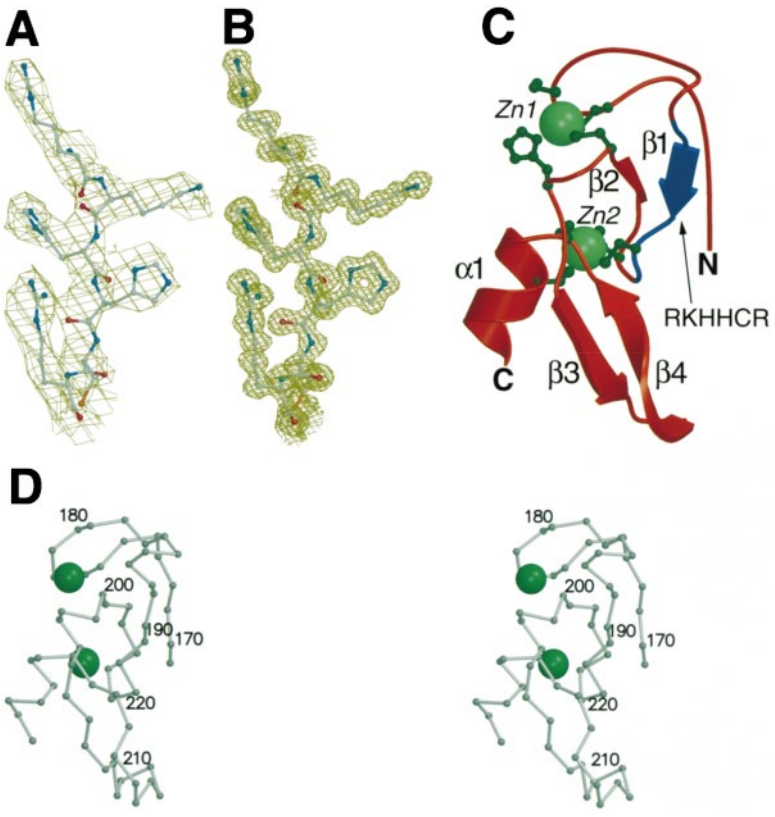


Figure 1. Structure of the Vps27p FYVE Domain

(A) Electron density contoured at 1.0 σ from a 3.2 Å density-modified MAD map. Residues 188 to 193 (top to bottom) are shown.

(B) Electron density contoured at 1.0 σ from a 1.15 Å $2F_o-F_c$ omit map showing the same residues as (A).

(C) The overall fold of the FYVE domain. Secondary structure elements are labeled. The zinc-liganding histidine and cysteine residues are shown in dark green. The location of the positive RKHHCR motif is colored blue.

(D) Stereoview of the Cα backbone. Figures were made using Molscript (Kraulis et al., 1991), Bobscript (Esnouf, 1997), and Raster3D (Merritt and Bacon, 1997).

Table 2. Refinement

| | |
|---|---|
| Resolution range | 30–1.15 Å |
| No. of reflections | 20,972 |
| R value[a] | 17.4% (21.3%) |
| $R_{free}$[b] | 18.1% (24.8%) |
| Luzatti coordinate error | 0.12 Å |
| Cross-validated Luzatti coordinate error | 0.13 Å |
| Bond length deviation | 0.012 Å |
| Bond angle deviation | 1.77° |
| Improper angle deviation | 1.03° |
| Dihedrals deviation | 23.6° |
| Average B factor | 12.6 Å$^2$ |
| Bonded main chain atom B factor rmsd | 1.6 Å$^2$ |
| Bonded side chain atom B factor rmsd | 3.4 Å$^2$ |
| Residues in most favored $\phi$–$\psi$ region | 89.8% |
| Residues in disallowed regions | 0.0% |

[a] $R = \Sigma(|F_{obs}| - k|F_{calc}|)/\Sigma|F_{obs}|$.
[b] $R_{free}$ is the R value calculated for a test set of reflections, comprising a randomly selected 5% of the data and not used during refinement.

one His and three Cys residues. The Vps27p His is atypical of the FYVE domain family. In most other FYVE sequences, this position is replaced by a Cys (Figure 2). Both Cys-176 and Cys-179 in the first ligand pair are in a $3_{10}$ helical conformation. Cys-200 and His-203 in the second pair are in an $\alpha$-helical conformation. The second $Zn^{2+}$-binding cluster consists of four Cys residues, 192, 195, 222, and 225. Both Cys pairs are in $\alpha$-helical conformations. The second pair forms the start of the C-terminal $\alpha$ helix (Figure 1C).

The molecular surface of the FYVE domain is dominated by a highly basic patch (Figure 3). A total of six positively charged side chains participate in the basic face. Five of these are from strand $\beta$1 or immediately adjoin it: Arg-188, Lys-189, His-190, His-191, and Arg-193. These residues are part of the conserved (R/K)(R/K) HHCR motif that is a defining feature of the FYVE domain. The sixth basic side chain, Arg-220, is contributed by $\beta$4. The N-terminal loop plays a supporting role in the basic patch, although it does not contain any positive charges. Trp-170 is at the edge of the patch and contributes one face of its indole ring to the flat surface. This Trp also buttresses the side chains of His-191 and Arg-193. Main chain groups and the side chain of Asp-172 stabilize the positions of positive charges. Gln-201 and Glu-217 also contribute to structural stabilization at the periphery of the basic patch. At the tip of the structure, past the edge of the main basic patch, Leu-185 and Leu-186 form a highly exposed hydrophobic protrusion that contrasts with the polar character of the rest of the surface.

### The (R/K)(R/K)HHCR Motif Forms a Basic Pocket

There is a small pocket of very concentrated positive charge at the center of the flat basic patch. This pocket is occupied by the two carboxylates from the C-terminal Asp (the last vector-derived residue) of a lattice-related molecule (Figure 4). The side chain carboxylate of the Asp occupies the most sterically occluded part of the pocket. The side chain makes close hydrogen bonds with the His-191 N$\delta$, His-191 main chain NH, and Arg-193 guanidino N$\eta$1. The C terminus carboxylate of the lattice-related molecule (residue V6′, where ′ denotes the symmetry-related molecule) occupies a less occluded site. It makes two short ($<$3.0 Å) and two long hydrogen bonds to charged groups and another close hydrogen bond to a tightly bound water molecule. The closest charge interactions are with Arg-193 N$\eta_2$ and His-190 N$\delta$; the longer interactions are with Arg-193 N$\eta_1$ and Arg-220 N$\epsilon$. The lattice contact with the basic pocket seems unquestionably unphysiological. It is described in detail here because it illustrates how a small acidic moiety—represented by the lattice-related C-terminal Asp—can accept no less than eight hydrogen bonds, six of them charged, all within a very small pocket.

Yet another charge pair is formed across the same lattice contact near, but outside, the basic pocket. Arg-188, the first Arg of the RKHHCR sequence of Vps27p, forms a salt bridge with Glu-V1′ from the C-terminal helix of the lattice contact molecule. Lys-189 also points in the direction of Glu-V1′, although it does not directly contact it. The V1′ subsite is about 8 Å away from the V6′ subsite, as judged by the distance separating the closest basic side chains in each subsite.

The crystals described here were obtained both in the presence and absence of a short chain (dibutyryl) PI3P. Even when the FYVE domain was crystallized in the presence of 5 mM PI3P under otherwise similar conditions, we failed to observe binding in the crystal. No crystals have thus far been obtained in different forms, either in the presence or absence of phosphoinositide. The lattice-related C-terminal helix occupies the expected binding site for PI3P. The binding of PI3P to the N-terminally extended form of the FYVE domain of Vps27p has been directly established by Burd and Emr (1998). The EEA1 counterpart of the short form of the Vps27p FYVE domain that was crystallized here is insufficient for subcellular targeting in vivo. The poorly conserved N-terminal extensions of at least some FYVE domains are thought to contribute to targeting through mechanisms that are not yet understood in detail but probably involve interactions with small G proteins or nonspecific membrane binding, or both. Neither the phosphoinositide binding of the minimal FYVE domains nor the binding of short chain phosphoinositides to either minimal or extended FYVE domains have been characterized in vitro. The key role of the conserved (R/K)(R/K)HHCR motif has been directly demonstrated based on mutagenesis of the motif in EEA1 (Burd and Emr, 1998). Replacement of these basic residues by Ala completely abolishes binding to PI3P (Burd and Emr, 1998). The crystal structure does not reveal any major roles for these basic residues in structural stabilization, so a direct interaction with PI3P is the only reasonable explanation for the mutagenic results. There can therefore be little doubt that our identification of the binding site is correct. These crystals are tightly packed, with $V_m = 2.0$ (Matthews, 1968). This crystal contact is only slightly larger than usual. The contact buries a combined total of 663 Å$^2$ of solvent-accessible surface area contributed by both molecules in the complex (1.4 Å probe). The PI3P-binding site lattice contact may be strengthened by the numerous partially buried charge interactions.

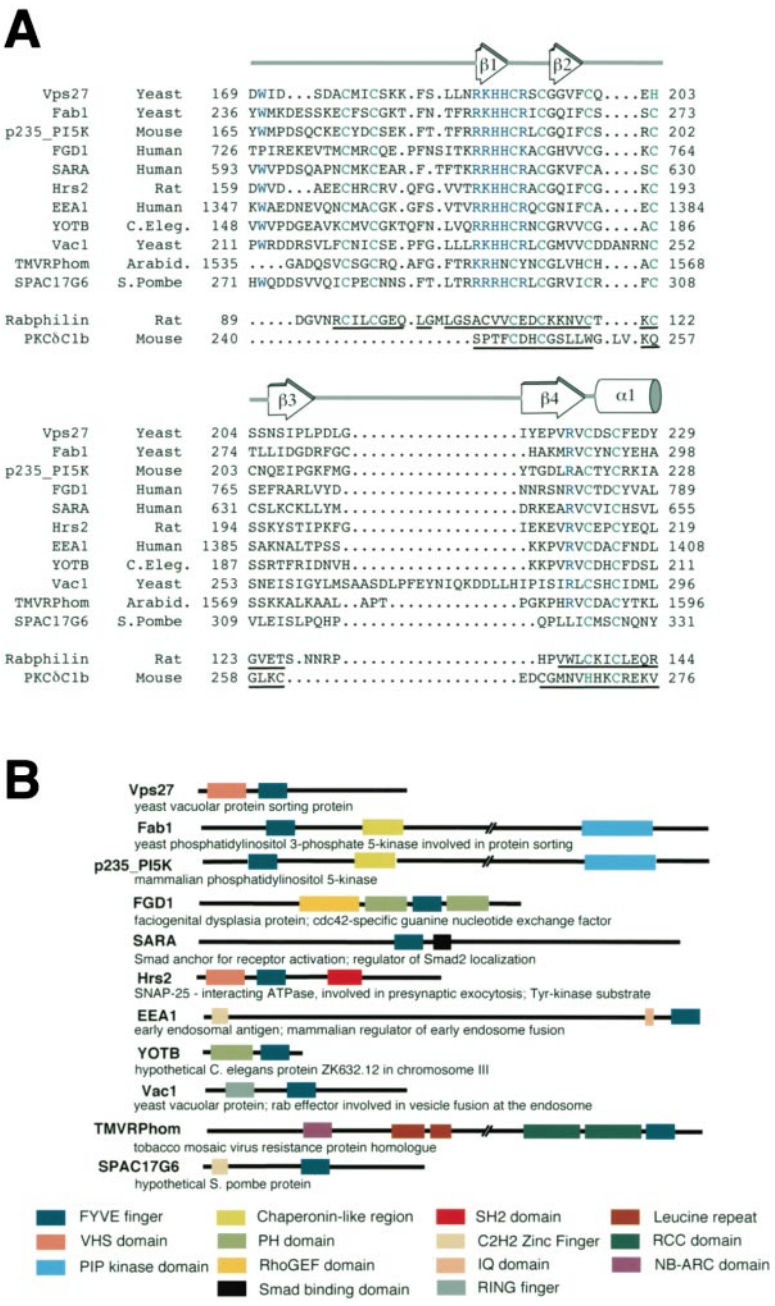


Figure 2. FYVE Domains

(A) Alignment of representative FYVE domains, the structurally homologous domain from rabphilin-3A, and the C1b domain of protein kinase Cδ. Secondary structure of Vps27p-FYVE is shown above the alignment. Residues that coordinate the $Zn^{2+}$ atoms are colored green, while residues that participate in the putative PI–3P binding pocket are colored blue. Residues in rabphilin and PKC that coincide with their counterparts in Vps27p (as determined by structural comparison) are underlined.

(B) Location of FYVE domains in the respective proteins. Other domains found in these proteins are shown. Domain information was obtained from Stenmark et al. (1996), Tsukazaki et al. (1998), Shisheva et al. (1999), and the Pfam database (Bateman et al., 1999). Sequences used in this figure were obtained from the following database entries: Vps27p, SwissProt VP27_YEAST; FAB1, SwissProt FAB1_YEAST (Yamamoto et al., 1995); p235_PI5K, GenBank AF102777 (Shisheva et al., 1999); FGD1, SwissProt FGD1_HUMAN (Pasteris et al., 1994); SARA, GenBank AF104304 (Tsukazaki et al., 1998); Hrs2, EMBL RNU87863_2 (Bean et al., 1997); EEA1, EMBL HSEEAP (Mu et al., 1995); YOTB, SwissProt YOTB_CAEEL; Vac1, SwissProt VAC1_YEAST (Weisman and Wickner, 1992); TMVRPhom, EMBL ATFCA1_116; SPAC17G6, EMBL SPAC17G6_14; rabphilin, SwissProt RP3A_RAT (Li et al., 1994); PKCδ-C1b, SwissProt KPCD_MOUSE (Mischak et al., 1991).

## Discussion

### Comparison to other $Zn^{2+}$-Binding Domains

Coordination of $Zn^{2+}$ by Cys and His residues is a fundamental mechanism for the stabilization of an otherwise very diverse group of proteins. Klug enumerated ten structurally distinct classes of “zinc fingers” as of the beginning of 1995 (Klug and Schwabe, 1995), and the number continues to grow. Many of the best known small $Zn^{2+}$-binding domains bind DNA, but many others do not. $Zn^{2+}$-binding domains can be classified by the number, type, and topology of their $Zn^{2+}$ ligands, their three-dimensional folds, and their functions. FYVE domains have been referred to as RING or “RING-FYVE” domains (Burd and Emr, 1998; Patki et al., 1998). The RING domains have the same predicted order in the primary sequence of the ligands for the two bound $Zn^{2+}$. The structure confirms that the arrangement of the $Zn^{2+}$ ligands in the primary structure is the same for FYVE and RING domains. The first $Zn^{2+}$ ion is coordinated by the first and third pairs, and the second ion is coordinated by the second and fourth pairs. The topology of the secondary structures around the second $Zn^{2+}$ ion is similar to that of the C3HC4 RING domain (Barlow et al., 1994), although the structures are not similar enough to superimpose. Contrary to some predictions, there is no apparent similarity to the fold of the PML RING domain (Borden et al., 1995). The similar pattern of $Zn^{2+}$ ligands in the primary structure is probably fortuitous.

The structure of the Vps27p FYVE domain confirms

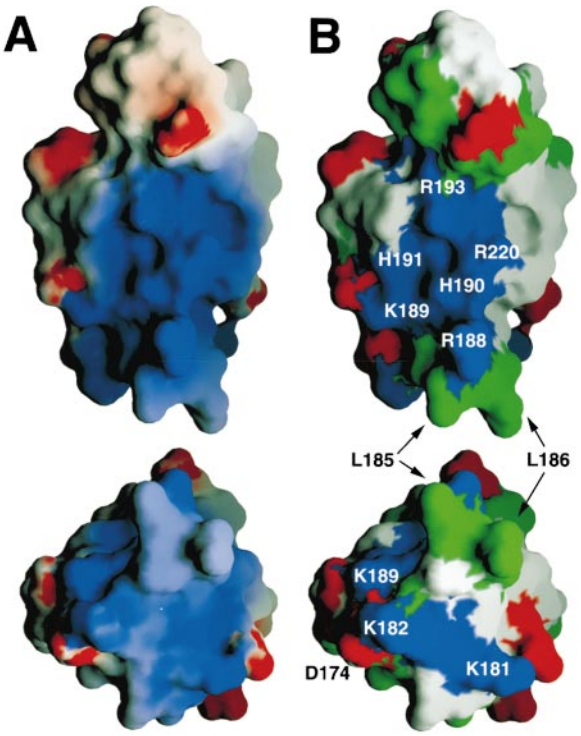


Figure 3. Molecular Surface of the FYVE Domain

The surfaces are colored by (A) electrostatic potential, with saturating color at ±5 kT/e, and (B) residue type: hydrophobic, green; basic, blue; acidic, red; and uncharged polar, white. Surfaces were drawn and colored using GRASP (Honig and Nicholls, 1995). The upper figures show the protein in sagittal projection, looking into the putative PI3P-binding site. The membrane-proximal end of the protein is at the bottom. The lower figures depict a view from the membrane normal into the protein. The PI3P-binding site is at the top.

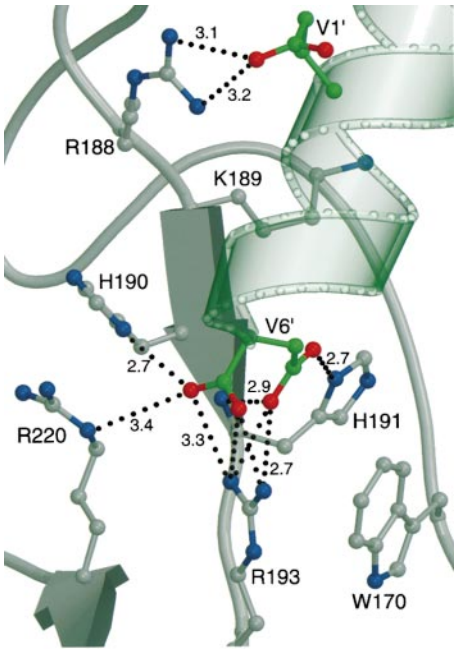


Figure 4. Lattice Contact with the PI3P-Binding Site

Close-up of interactions between the PI3P-binding site and the symmetry-related C-terminal helix (translucent green). Residues from the symmetry-related molecule (designated by primes) are colored green. Putative hydrogen-bonding interactions are shown along with corresponding interatomic distances in angstroms. To maintain clarity, some interatomic distances are not shown. The figure was drawn using Molscript and Raster3D.

the proposed link between the FYVE domains and the class of $Zn^{2+}$-binding domains found in rabphilins, a family of membrane-interacting effectors for the Rab small G proteins (Stenmark et al., 1996; Ostermeier and Brünger, 1999). Both $Zn^{2+}$ ions and 44 out of 61 FYVE domain residues can be superimposed on their counterparts in the three-dimensional structure of rabphilin-3A. These 44 residues superimpose with an rms deviation of 1.2 Å. With the exception of the seven equivalent $Zn^{2+}$-binding Cys residues, only 3 out of 44 residues are identical in the two proteins. Cys-122 of rabphilin-3A is replaced by His-203 in Vps27p, which coordinates the $Zn^{2+}$ ions through its Nδ. The only apparent effect of this change is to push the His-203 Cα 0.4 Å further away from the $Zn^{2+}$ ion as compared to the rabphilin Cys-122.

The differences between the rabphilin $Zn^{2+}$-binding domain and the FYVE domain are concentrated in three regions. The six N-terminal residues 169–174 of the FYVE domain include a loop that is pulled away from the first β sheet. In contrast, this part of the rabphilin $Zn^{2+}$-binding domain includes the C terminus of the long α1 helix and its link to the core of the $Zn^{2+}$-binding domain. These differences are likely to be important because Trp-170, Asp-172, and the main chain of this section help stabilize the FYVE domain residues that make up the basic pocket.

Residues 185 and 186 of the FYVE domain comprise an unusual highly exposed hydrophobic protrusion in the FYVE domain structure. The rabphilin-3A sequence is one residue longer than that of the FYVE domain in this region (Figure 2), which immediately precedes β1. The corresponding rabphilin residues 103–105 are also exposed hydrophobics, but they are in a different conformation from that in the FYVE domain. These rabphilin residues have temperature factors (B factors) of 90–100 $Å^2$ as compared to ~10 $Å^2$ in the FYVE domain structure. The absolute differences in B factors probably overstate the real structural differences, since the average B factors of the two structures are quite different. The average B factors for the two structures are 35.1 $Å^2$ and 12.6 $Å^2$, respectively. Taken in proportion to the entire structure, this region is three times more mobile in rabphilin-3A than in the Vps27p FYVE domain. The structural differences may reflect, at least in part, the higher mobility of this part of the rabphilin structure or the looser packing of the rabphilin-3A/Rab3A crystal rather than real functional differences.

The last region of difference is in the β3–β4 loop. In both structures, this region is pulled away from the rest of the domain; however, the similarity ends there. This region of rabphilin-3A is also extremely mobile. Residues 128–133 of rabphilin-3A have temperature factors in the 90–110 $Å^2$ range, while the corresponding figures for this region of the FYVE domain are 6–14 $Å^2$. It is sometimes assumed that conformational differences involving high mobility regions have little functional meaning. In the case of this loop, there is nevertheless good

reason to expect the conformational differences are functionally significant. The conformation observed in the FYVE domain clashes with the C-terminal two residues of Rab3A as bound to rabphilin. It seems clear that the β3–β4 loop of rabphilin cannot move into the conformation observed in the FYVE domain, at least not while bound to Rab3A.

There are substantial structural similarities between the FYVE domain and at least three other classes of small $Zn^{2+}$-binding domains. The five core secondary structural elements (β1–β4, α1) and the second $Zn^{2+}$-binding site are superimposable with the $Zn^{2+}$-containing DNA-binding domain of GATA-1 (Omichinski et al., 1993), the C1 domain of protein kinase C (Zhang et al., 1995), and the LIM domain (Perez-Alvarado et al., 1996). Twenty-nine to thirty-two residues are superimposable with an rms deviation of 1.4 to 1.8 Å. These similarities were too weak to score as significant in a VAST search of the Protein Data Bank (Gibrat et al., 1996). These similarities fall within the "twilight zone" of weak structural similarity, and it is possible they represent nothing more than chance. There is no known functional similarity between the FYVE domain and GATA-1 or the LIM domain. In light of the similar function of the FYVE and C1 (Hurley et al., 1997) domains in membrane targeting, it is tempting to postulate a meaningful connection between these two.

### Phosphatidylinositol 3-Phosphate-Binding Site and Specificity

One of the most remarkable properties of the FYVE motif is that so small a protein domain can form a highly specific ligand-binding pocket. How does a tiny domain form a specificity pocket? The structure of the basic pocket of the FYVE domain suggests an answer. The basic pocket is built on top of the edge of the first β strand (β1). The main chain NH of His-191 points directly into the pocket, providing one ligand. The consecutive His residues 190 and 191 flank the pocket. The β structure positions these opposite to each other. Because the β strand participates in the pocket edge-on, the side chains of both His residues are exposed on the same face of the molecule. Because the His side chain is the shortest of the three basic amino acids, these side chains are both within charge interaction distance of a single dianionic ligand. This could be either Asp-$COO^-$, as seen in the crystals, or a phosphate group, in the case of the physiological ligand. Arg-193 is positioned two residues away. This puts enough distance between its Cα and the pocket that the guanidino group can reach with the side chain in a fully extended conformation. This pocket is a nearly perfect phosphate-binding site, yet it is too sterically restricted to bind the 1-phosphate of PI3P. We therefore expect that it is the 3-phosphate-binding site.

The side chain of Glu-V1′ is 9 Å from the Asp-V6′ carboxylate. This is just slightly greater than the 7 Å between the 1- and 3-phosphates of PI3P. We have modeled the PI3P headgroup so that the 1-phosphate forms a salt bridge with Arg-188 in the same way as the lattice-related Glu-V1′ does in the crystal (Figure 5). This model resembles the binding of inositol (1,4,5)trisphosphate ($IP_3$) to the PH domain of phospholipase C-δ1

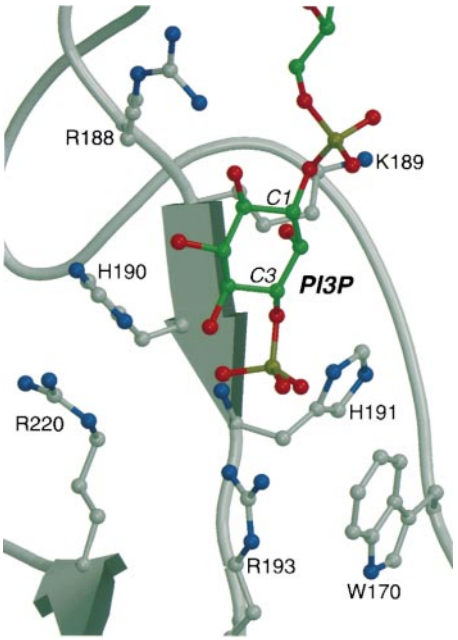


Figure 5. Model for PI3P Headgroup Binding to the RKHHCR Motif of the FYVE Domain

A PI3P model was energy minimized using Quanta (Molecular Simulations, Inc.) and oriented near the protein surface to favor hydrogen bonding while avoiding steric clashes. The C-terminal helix of the symmetry-related molecule (Figure 4) was used as a guide. The orientation of the protein is identical to that in Figure 4. The figure was drawn using Molscript and Raster3D.

(Ferguson et al., 1995). In the $IP_3$/PH domain complex, the 4- and 5-phosphates interact with a deep pocket via an extensive network of charged interactions and hydrogen bonds. In contrast, the 1-phosphate is outside the pocket and accepts a single hydrogen bond.

How can we rationalize the exacting specificity of the FYVE domain for PI3P to the exclusion of closely related phosphoinositides? Despite the lack of bound PI3P in these crystals, the lattice-supplied anionic ligand uses similar interactions. Its binding mode suggests a reasonable explanation for the observed stereospecificity. The basic pocket is too small to bind an inositol bis- or trisphosphate, so the absence of binding to PI(3,4)$P_2$, PI(4,5)$P_2$, PI(3,5)$P_2$, and $PIP_3$ is not surprising. As for the singly phosphorylated phosphoinositides, there are no reports that binding of PI(5)P to FYVE domains has been tested. The available structural and functional data are insufficient to rule out the possibility that FYVE domains could bind this scarce lipid. The spacing between the 1- and 3-phosphate subsites is incompatible with the longer distance between the 1- and 4-phosphates of PI(4)P, consistent with the lack of binding of this lipid.

The Trp-170, RKHHCR sequence, and Arg-220 of the PI3P-binding site are conserved throughout the FYVE domains, consistent with a common function for all FYVE domains in PI3P binding. These residues are absent in the rabphilin $Zn^{2+}$-binding domain, despite the similarity in its fold. This leads us to predict that the rabphilin $Zn^{2+}$-binding domain does not bind PI3P. Indeed, the molecular surface of the rabphilin $Zn^{2+}$-binding domain that corresponds to the PI3P-binding site

of the FYVE domain is not basic, suggesting that the rabphilin $Zn^{2+}$-binding domain does not specifically bind to phosphoinositides at all.

The PI3P interaction occurs on one side of the domain as it docks onto the membrane rather than on the most membrane-proximal tip of the domain. This "sideways" mode of interaction is reminiscent of the active site of PIPK (Rao et al., 1998) and of the $PIP_2$ binding mechanism of the phospholipase Cδ PH domain (Ferguson et al., 1995), although it is quite different from many other membrane-targeting domains and surface-active enzymes (Hurley and Grobler, 1997). The unusual nature of these interactions is consistent with their specificity for the most membrane-distal moieties of phosphoinositides. The 3, 4, and 5 positions of the large and highly polar phosphatidylinositol headgroup probably protrude several angstroms above the surrounding smaller headgroups of other phospholipids in the membrane. The spacing between the nonspecific membrane–interacting elements and the specific phosphate recognition pocket could be considered a molecular ruler and may itself be a central factor in controlling specificity.

**Membrane-Targeting Mechanism**

Regulated membrane targeting plays a central role in many, if not most, cell signaling pathways. The FYVE domain is the most recent addition to a growing family of domains and motifs that target signal-transducing proteins to cell membranes. Some of these domains target by means of protein–protein interactions with integral membrane proteins (Pawson and Scott, 1997). Other domains target membranes by means of direct interactions with membrane lipids (Hurley and Grobler, 1997), and still others use some combination of protein- and lipid-directed mechanisms. The C1, C2, and PH domains (Hurley and Grobler, 1997), the myristoyl-$Ca^{2+}$ and myristoyl-electrostatic switch motifs (Murray et al., 1997), and now the FYVE domain are examples of membrane lipid–directed targeting mechanisms with widespread roles in eukaryotic cell signaling.

Analysis of the hydrophobic and basic surfaces at the membrane-proximal tip of the FYVE domain structure suggests a role for nonspecific bilayer interactions. The hydrophobic protrusion formed by Leu-185 and Leu-186 is predicted to be membrane proximal and could be a site for hydrophobic penetration into the bilayer. This hydrophobic structure is conserved among other FYVE domains. This hydrophobic patch is relatively small, suggesting that hydrophobic interactions are unlikely to be a major driving force for membrane binding. Lys-181 and Lys-182 are near the predicted plane of the membrane but on the opposite side of the FYVE domain from the PI3P-binding pocket. These positively charged residues are only weakly conserved, although most FYVE domain sequences have some positive charges in the same area of the three-dimensional structure. The presence of the positive charges suggests that weak nonspecific electrostatic interactions may play a secondary role in FYVE domain–membrane interactions but are unlikely to be a major driving force. The limited role for nonspecific interactions with the membrane should facilitate the rapid dissociation of FYVE domain–targeted proteins following turnover of PI3P. The structure is consistent with the observation that specific PI3P binding is the major driving force for interaction with the membrane (Burd and Emr, 1998; Gaullier et al., 1998; Patki et al., 1998).

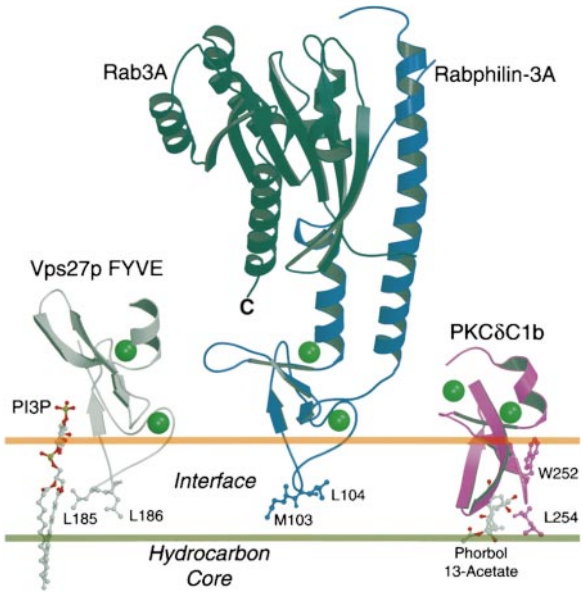


Figure 6. Membrane Interaction Model

The Vps27p FYVE domain, rabphilin-3A/Rab3A complex (Brünger et al., 1999), and the C1b domain of protein kinase Cδ (Zhang et al., 1995), shown in the predicted membrane-bound orientation (sagittal projection). Orientations of rabphilin-3A/Rab3A and PKCδ-C1b are based on structural alignments with the Vps27p-FYVE. Hydrophobic ligands and residues that may be important for membrane interactions are shown. The membrane is divided according to the model of Wiener and White (1992; White and Wimley, 1994), which describes the distribution of lipid and protein functional groups within the bilayer. The interfacial region, containing water, lipid headgroups, glycerol, carbonyl, and methylene groups, constitutes the outer quarters of the membrane; the central half of the membrane is occupied by a hydrocarbon core, containing the lipid fatty acid chains. The interfacial zone of the membrane is depicted to scale with a thickness of 15 Å. We have inserted the proteins to reasonable depths in the membrane. The C-terminal end of the ordered part of the solved Rab3A structure is labeled; the C terminus of the full-length protein is geranyl geranylated. In the orientation shown, the Rab3A C terminus is near enough to the membrane surface that a covalently attached geranyl–geranyl moiety can penetrate into the membrane. Structures were drawn using Molscript and Raster3D.

**Parallels in Membrane Targeting by FYVE Domains, C1 Domains, and Rabphilin**

The structural similarity between the FYVE and C1 domains suggests analogies between their mechanisms of regulated membrane targeting. The typical C1 domains target protein kinase Cs and other signal-transducing proteins to diacylglycerol-containing membranes (Hurley et al., 1997). When the FYVE and C1 structures are superimposed, the Leu-185/Leu-186 hydrophobic protrusion of the FYVE domain overlaps with the parts of the C1 domain that have been shown to penetrate lipid bilayers (Figure 6; Zhang et al., 1995; Xu et al., 1997). The basic patch of the FYVE coincides with a basic surface on the C1 domain that is thought to interact with phosphatidylserine and other acidic phospholipid headgroups. This suggests that both the FYVE and C1

domains interact with membranes by analogous nonspecific interactions and with similar geometry, despite completely different specific interactions.

The FYVE domain–containing protein EEA1 is an effector of the small G protein Rab5. Could EEA1 interact with Rab5 by the same mechanism demonstrated for rabphilin and Rab3A (Ostermeier and Brünger, 1999)? The steric conflicts caused by the differences in the β3–β4 loop argue against a precisely equivalent mechanism. Further, the critical Rab3A-binding SGAWFF motif of rabphilin is completely absent in FYVE domain proteins. On the other hand, there is some homology between the N-terminal extensions of some FYVE domains (omitted in this structure) and the N-terminal Rab3A-binding helix of rabphilin. The FYVE domain can be docked onto a model membrane based on the PI3P-binding pocket. If the rabphilin/Rab3A complex is overlaid on the membrane-docked FYVE domain, the entire Rab3A molecule as found in the solved structure is quite distant from the membrane (Figure 6). The C-terminal site of geranyl geranylation on Rab3A is 26 residues C-terminal to the last ordered residue in the structure of the Rab3A/rabphilin complex. The last ordered residues of Rab3A point in the direction of the membrane. If the polypeptide chain were to continue in the same direction, the additional 26 residues are ample to reach the predicted bilayer surface. This model is attractive, since it would position the geranyl–geranyl group perfectly for interaction with the bilayer. Some minor repositioning of the C terminus of the small G protein and/or the β3–β4 loop would be required to avoid steric conflicts. This structural model is consistent with the recently proposed dual targeting model for EEA1 by Rab5 and PI3P (Wiedemann and Cockroft, 1998).

The modeled membrane interactions suggest that three different classes of $Zn^{2+}$-binding domains all insert tip down into bilayers. The insertion mechanism for the protein kinase C C1 domain has already been directly confirmed by NMR studies in short-chain lipid micelles (Xu et al., 1997). The models make testable predictions about the roles of conserved hydrophobic residues in stabilizing membrane binding by FYVE domains and rabphilins. The models place the exposed hydrophobic Met–Leu sequence on rabphilin-3A in contact with the membrane, as for the Leu-185/Leu-186 sequence of the Vps27p FYVE domain. These unexpected similarities in detail lend confidence to the idea that all of these domains interact with membrane bilayers in similar ways, yet with quite different specificities and biological effects.

## Experimental Procedures

### Protein Expression and Purification

Vps27p residues 155–229 were amplified using PCR and cloned into the BamHI and EcoRI sites of pGEX-2T (Smith and Johnson, 1988; Amersham-Pharmacia). The vector contributes the sequence EFIVTD at the C terminus and a glycine residue at the N terminus of the predicted thrombin cleavage product of the fusion protein. The GST-fusion protein was expressed in BL21(DE3) cells (Novagen) and batch purified from lysate using glutathione–Sepharose resin (Amersham-Pharmacia). Sepharose beads were washed successively with 10 vol 1 M NaCl/1×PBS (pH 7.5) and 1×PBS (pH 7.5). The fusion protein was cleaved from the beads by overnight incubation with thrombin (Roche). The postcleavage supernatant was concentrated to <10 ml and loaded onto a Superdex 200 (26/60) gel filtration column (Amersham-Pharmacia) equilibrated with 0.5 M NaCl/0.1 M triethanolamine (pH 7.5) on an FPLC system (Amersham-Pharmacia). The cleaved protein eluted as a monomer and was concentrated and stored at −80°C in equilibration/elution buffer with 20% glycerol. Protein yield was 6 mg/l bacterial culture. MALDI-TOF mass spectrometry (Perseptive Voyager-DE) indicated that the sample used for crystallization was an equal mixture of proteins consisting of residues 163–229 and 164–229, respectively, along with six residues with the sequence EFIVTD derived from the vector at the C terminus. Stoichiometric binding of 2 mol $Zn^{2+}$/mol protein was confirmed by colorimetric assay (Giedroc et al., 1986).

### Protein Crystallization

Freshly thawed protein was dialyzed into low-salt buffer (50 mM NaCl/20 mM Tris-HCl [pH 7.5], 10 mM DTT) and concentrated to 13–15 mg/ml. Two crystal forms were obtained by hanging drop diffusion at 4°C using Hampton Research sparse matrix screens (Jancarik and Kim, 1991). Small crystals (100 × 30 × 5 μm) appeared overnight in 0.1 M HEPES (pH 6.5–7.5), 60%–70% MPD. These crystals diffracted to 2.6 Å on a laboratory source. Larger crystals (500 × 200 × 25 μm) grew in 5–6 days in 0.2 M ammonium acetate, 0.1 M sodium acetate (pH 4.6), 15% PEG 4000. These diffracted to as high as 1.7 Å on a laboratory source and 1.15 Å at beamline X9B, National Synchrotron Light Source (NSLS) and were used for structure determination and refinement.

### Crystallographic Data Collection

Crystals were soaked for 10 min each in 0.1 M ammonium acetate, 0.1 M sodium acetate (pH 4.6), 10% PEG 4000, and 15%, 20%, and 25% glycerol. Cryoprotected crystals were frozen by immersion in liquid propane. Initial data were collected using mirror-focused Cu Kα radiation from a Rigaku RU-200 rotating anode source at 100 mA/50 kV and a RAXIS-IV image plate detector. Data were collected in 1° oscillation frames at 30 min per frame at 95 K. The crystals are in space group P1 with unit cell dimensions and angles a = 24.1 Å, b = 26.5 Å, c = 31.8 Å, α = 112.0°, β = 92.5°, γ= 105.7°, as determined by autoindexing using HKL (Otwinowski and Minor, 1997). Taking advantage of the intrinsic $Zn^{2+}$ bound to the native protein, MAD data were collected at beamline X9B using three wavelengths around the Zn K edge (Table 1). MAD data were collected in 3° oscillation frames at 180 s per frame, at 95 K, using an ADSC CCD detector (Area Detector Systems Corp., San Diego). Subsequently, a higher resolution 1.15 Å data set was collected at beamline X9B under the same conditions. Synchrotron data were indexed and merged using HKL.

### Structure Determination and Refinement

The positions of the $Zn^{2+}$ atoms were determined, heavy atom parameters were refined, and MAD phases calculated using SOLVE (Terwilliger, 1994a, 1994b; Terwilliger and Berendzen, 1996). The electron density map calculated from the initial phases was solvent flattened in DM (Cowtan, 1994) using a solvent fraction of 0.35. The resulting 3.2 Å resolution electron density map was used to build an atomic model in O (Jones et al., 1991). Model refinement was carried out with CNS using torsional dynamics and the maximum likelihood target function (Brünger et al., 1998). The stereochemical restraints of Engh and Huber (1991) and the individual thermal factor restraints of Tronrud (1996) were used. The refinement was monitored using the free R factor calculated with 5% of observed reflections (Brünger, 1992). The refined crystal structure includes residues 169–229 of Vps27p, residues V1–V6 derived from the vector, and 111 water molecules. PROCHECK (Laskowski et al., 1993) was used to gauge the stereochemical quality of the final model, which scores as well as expected at 1.15 Å resolution. There are no non-Gly residues in the disallowed or generously allowed regions of the Ramachandran plot.

## Acknowledgments

We thank Scott Emr and Chris Burd for contributions to early stages of this project, discussions, and providing DNA, and Zbyszek Dauter and Yosuke Tsujishita for assistance with data collection at beamline

X9B, National Synchrotron Light Source, Brookhaven National Laboratories.

Received March 16, 1999; revised April 26, 1999.

**References**

Barlow, P.N., Luisi, B., Milner, A., Elliott, M., and Everett, R. (1994). Structure of the C3HC4 domain by $^1$H-nuclear magnetic resonance spectroscopy. J. Mol. Biol. *237*, 201–211.

Bateman, A., Birney, E., Durbin, R., Eddy, S.R., Finn, R.D., and Sonnhammer, E.L. (1999). Pfam 3.1: 1313 multiple alignments match the majority of proteins. Nucleic Acids Res. *27*, 260–262.

Bean, A.J., Seifert, R., Chen, Y.A., Sacks, R., and Scheller, R.H. (1997). Hrs-2 is an ATPase implicated in calcium-regulated secretion. Nature *385*, 826–829.

Borden, K.L., Boddy, M.N., Lally, J., O'Reilly, N.J., Martin, S., Howe, K., Solomon, E., and Freemont, P.S. (1995). The solution structure of the RING finger domain from the acute promyelocytic leukemia proto-oncoprotein PML. EMBO J. *14*, 1532–1541.

Brünger, A.T. (1992). The free R value: a novel statistical quantity for assessing the accuracy of crystal structures. Nature *355*, 472–474.

Brünger, A.T., Adams, P.D., Clore, G.M., DeLano, W.L., Gros, P., Grosse-Kunstleve, R.W., Jiang, J.S., Kuszewski, J., Nilges, M., Pannu, N.S., et al. (1998). Crystallography and NMR system (CNS): a new software system for macromolecular structure determination. Acta Crystallogr. D *54*, 905–921.

Burd, C.G., and Emr, S.D. (1998). Phosphatidylinositol(3)-phosphate signaling mediated by specific binding to RING FYVE domains. Mol. Cell *2*, 157–162.

Christoforidis, S., McBride, H.M., Burgoyne, R.D., and Zerial, M. (1999). The Rab5 effector EEA1 is a core component of endosome docking. Nature *397*, 621–626.

Corvera, S., and Czech, M.P. (1998). Direct targets of phosphoinositide 3-kinase products in membrane traffic and signal transduction. Trends Cell Biol. *8*, 442–446.

Cowtan, K. (1994). "dm": an automated procedure for phase improvement by density modification. Joint CCP4 ESF-EACBM Newslett. Protein Crystallogr. *31*, 34–38.

De Camilli, P., Emr, S.D., McPherson, P.S., and Novick, P. (1996). Phosphoinositides as regulators in membrane traffic. Science *271*, 1533–1539.

Engh, R., and Huber, R. (1991). Accurate bond and angle parameters for X-ray protein-structure refinement. Acta Crystallogr. A *47*, 392–400.

Esnouf, R.M. (1997). An extensively modified version of MolScript that includes greatly enhanced coloring capabilities. J. Mol. Graph. Model. *15*, 132–134.

Ferguson, K.M., Lemmon, M.A., Schlessinger, J., and Sigler, P.B. (1995). Structure of the high affinity complex of inositol trisphosphate with a phospholipase C pleckstrin homology domain. Cell *83*, 1037–1046.

Fruman, D.A., Meyers, R.E., and Cantley, L.C. (1998). Phosphoinositide kinases. Annu. Rev. Biochem. *67*, 481–507.

Gary, J.D., Wurmser, A.E., Bonangelino, C.J., Weisman, L.S., and Emr, S.D. (1998). Fab1p is essential for PtdIns(3)P 5-kinase activity and the maintenance of vacuolar size and membrane homeostasis. J. Cell Biol. *143*, 65–79.

Gaullier, J.-M., Simonsen, A., D'Arrigo, A., Bremnes, B., and Stenmark, H. (1998). FYVE fingers bind PtdIns(3)P. Nature *394*, 432–433.

Gibrat, J.-F., Madej, T., and Bryant, S.H. (1996). Surprising similarities in structure comparison. Curr. Opin. Struct. Biol. *6*, 377–385.

Giedroc, D.P., Keating, K.M., Williams, K.R., Konigsberg, W.H., and Coleman, J.E. (1986). Gene *32* protein, the single-stranded DNA binding protein from bacteriophage T4, is a zinc metalloprotein. Proc. Natl. Acad. Sci. USA *83*, 8452–8456.

Hendrickson, W.A. (1991). Determination of macromolecular structure from anomalous diffraction of synchrotron radiation. Science *254*, 51–58.

Honig, B., and Nicholls, A. (1995). Classical electrostatics in biology and chemistry. Science *268*, 1144–1149.

Hurley, J.H., and Grobler, J.A. (1997). Protein kinase C and phospholipase C: bilayer interactions and regulation. Curr. Opin. Struct. Biol. *7*, 557–565.

Hurley, J.H., Newton, A.C., Parker, P.J., Blumberg, P.M., and Nishizuka, Y. (1997). Taxonomy and function of C1 protein kinase C homology domains. Protein Sci. *6*, 477–480.

Irvine, R.F. (1998). Inositol phospholipids: translocation, translocation, translocation... Curr. Biol. *8*, R557–R559.

Jancarik, J., and Kim, S.-H. (1991). Sparse matrix sampling: a screening method for crystallization of proteins. J. Appl. Crystallogr. *24*, 409–411.

Jones, T.A., Zou, J.Y., Cowan, S.W., and Kjeldgaard, M. (1991). Improved methods for building protein models in electron density maps and the location of errors in these models. Acta Crystallogr. A *47*, 110–119.

Klug, A., and Schwabe, J.W.R. (1995). Protein motifs 5. Zinc fingers. FASEB J. *9*, 597–604.

Kraulis, P. (1991). MOLSCRIPT: a program to produce both detailed and schematic plots of protein structures. J. Appl. Crystallogr. *24*, 946–950.

Laskowski, R.A., MacArthur, M.W., Moss, D.S., and Thornton, J.M. (1993). PROCHECK: a program to check the stereochemical quality of protein structures. J. Appl. Crystallogr. *24*, 946–950.

Li, C., Takei, K., Geppert, M., Daniell, L., Stenius, K., Chapman, E.R., Jahn, R., De Camilli, P., and Südhof, T.C. (1994). Synaptic targeting of rabphilin-3A, a synaptic vesicle $Ca^{2+}$/phospholipid-binding protein, depends on rab3A/3C. Neuron *13*, 885–898.

Matthews, B.W. (1968). Solvent content of protein crystals. J. Mol. Biol. *33*, 491–497.

Merritt, E.A., and Bacon, D.J. (1997). Raster3D version 2.0: a program for photorealistic molecular graphics. Methods Enzymol. *277*, 505–524.

Mischak, H., Bodenteich, A., Kolch, W., Goodnight, J., Hofer, F., and Mushinski, J.F. (1991). Mouse protein kinase C-delta, the major isoform expressed in mouse hemopoietic cells: sequence of the cDNA, expression patterns, and characterization of the protein. Biochemistry *30*, 7925–7931.

Mu, F.T., Callaghan, J.M., Steele-Mortimer, O., Stenmark, H., Parton, R.G., Campbell, P.L., McCluskey, J., Yeo, J.P., Tock, E.P., and Toh, B.H. (1995). EEA1, an early endosome-associated protein. EEA1 is a conserved alpha-helical peripheral membrane protein flanked by cysteine "fingers" and contains a calmodulin-binding IQ motif. J. Biol. Chem. *270*, 13503–13511.

Murray, D., Ben-Tal, N., Honig, B., and McLaughlin, S. (1997). Electrostatic interaction of myristoylated proteins with membranes: simple physics, complicated biology. Structure *5*, 985–989.

Odorizzi, G., Babst, M., and Emr, S.D. (1998). Fab1p PtdIns(3)P 5-kinase function essential for protein sorting in the multivesicular body. Cell *95*, 847–858.

Omichinski, J.G., Clore, G.M., Schaad, O., Felsenfeld, G., Trainor, C., Appella, E., Stahl, S.J., and Gronenborn, A.M. (1993). NMR structure of a specific DNA complex of Zn-containing DNA binding domain of GATA-1. Science *261*, 438–446.

Ostermeier, C., and Brünger, A.T. (1999). Structural basis of Rab effector specificity: crystal structure of the small G protein Rab3A complexed with the effector domain of rabphilin-3A. Cell *96*, 363–374.

Otwinowski, Z., and Minor, W. (1997). Processing of X-ray diffraction data collected in oscillation mode. Methods Enzymol. *276*, 307–326.

Pasteris, N.G., Cadle, A., Logie, L.J., Porteous, M.E., Schwartz, C.E., Stevenson, R.E., Glover, T.W., Wilroy, R.S., and Gorski, J.L. (1994). Isolation and characterization of the faciogenital dysplasia (Aarskog-Scott syndrome) gene: a putative Rho/Rac guanine nucleotide exchange factor. Cell *79*, 669–678.

Patki, V., Virbasius, J., Lane, W.S., Toh, B.-H., Shpetner, H.S., and Corvera, S. (1997). Identification of an early endosomal protein regulated by phosphatidylinositol 3-kinase. Proc. Natl. Acad. Sci. USA *94*, 7326–7330.

Patki, V., Lawe, D.C., Corvera, S., Virbasius, J.V., and Chawla, A. (1998). A functional PtdIns(3)P binding motif. Nature *394*, 433–434.

Pawson, T., and Scott, J.D. (1997). Signaling through scaffold, anchoring, and adaptor proteins. Science *278*, 2075–2080.

Perez-Alvarado, G.C., Kosa, J.L., Louis, H.A., Beckerle, M.C., Winge, D.R., and Summers, M.F. (1996). Structure of the cysteine-rich intestinal protein, CRIP. J. Mol. Biol. *257*, 153–174.

Piper, R.C., Cooper, A., Yang, H., and Stevens, T.H. (1995). VPS27 controls vacuolar and endocytic traffic through a prevacuolar compartment in Saccharomyces cerevisiae. J. Cell Biol. *131*, 603–617.

Rao, V.D., Misra, S., Boronenkov, I.V., Anderson, R.A., and Hurley, J.H. (1998). Structure of type IIβ phosphatidylinositol phosphate kinase: a protein kinase fold flattened for interfacial phosphorylation. Cell *94*, 829–839.

Shisheva, A., Sbrissa, D., and Ikonomov, O. (1999). Cloning, characterization, and expression of a novel $Zn^{2+}$-binding FYVE finger containing phosphoinositide kinase in insulin-sensitive cells. Mol. Cell. Biol. *19*, 623–634.

Simonsen, A., Lippe, R., Christoforidis, S., Gaullier, J.-M., Brech, A., Callaghan, J., Toh, B.-H., Murphy, C., Zerial, M., and Stenmark, H. (1998). EEA1 links PI(3)K function to Rab5 regulation of endosome fusion. Nature *394*, 494–498.

Smith, D.B., and Johnson, K.S. (1988). Single-step purification of polypeptides expressed in *Escherichia coli* as fusions with glutathione S-transferase. Gene *67*, 31–40.

Stenmark, H., Asaland, R., Toh, B., and D'Arrigo, A. (1996). Endosomal localization of the autoantigen EEA1 is mediated by a zinc-binding FYVE finger. J. Biol. Chem. *271*, 24048–24054.

Terwilliger, T.C. (1994a). MAD phasing: Bayesian estimates of $F_A$. Acta Crystallogr. D *50*, 11–16.

Terwilliger, T.C. (1994b). MAD phasing: treatment of dispersive differences as isomorphous replacement information. Acta Crystallogr. D *50*, 17–23.

Terwilliger, T.C., and Berendzen, J. (1996). Correlated phasing of multiple isomorphous replacement data. Acta Crystallogr. D *52*, 749–757.

Toker, A., and Cantley, L.C. (1997). Signalling through the lipid products of phosphoinositide 3-OH kinase. Nature *387*, 673–676.

Tronrud, D.E. (1996). Knowledge-based B-factor restraints for the refinement of proteins. J. Appl. Crystallogr. *29*, 100–104.

Tsukazaki, T., Chiang, T.A., Davison, A.F., Attisano, L., and Wrana, J.L. (1998). SARA, a FYVE domain protein that recruits Smad2 to the TGF-β receptor. Cell *95*, 779–791.

Weisman, L.S., and Wickner, W. (1992). Molecular characterization of VAC1, a gene required for vacuole inheritance and vacuole protein sorting. J. Biol. Chem. *267*, 618–623.

White, S.H., and Wimley, W.C. (1994). Peptides in lipid bilayers: structural and thermodynamic basis for partitioning and folding. Curr. Opin. Struct. Biol. *4*, 79–86.

Wiedemann, C., and Cockroft, S. (1998). Sticky fingers grab a lipid. Nature *394*, 426–427.

Wiener, M.C., and White, S.H. (1992). Structure of a fluid dioleoylphosphatidylcholine bilayer determined by joint refinement of x-ray and neutron diffraction data. III. Complete structure. Biophys. J. *61*, 434–447.

Wurmser, A.E., Gary, J.D., and Emr, S.D. (1999). Phosphoinositide 3-kinases and their FYVE domain-containing effectors as regulators of vacuolar/lysosomal membrane trafficking pathways. J. Biol. Chem. *274*, 9129–9132.

Xu, R.X, Pawelczyk, T., Xia, T.-H., and Brown, S.C. (1997). NMR structure of a protein kinase C-phorbol-binding domain and study of protein-lipid micelle interactions. Biochemistry *36*, 10709–10717.

Yamamoto, A., DeWald, D.B., Boronenkov, I.V., Anderson, R.A., Emr, S.D., and Koshland, D. (1995). Novel PI(4)P 5-kinase homologue, Fab1p, essential for normal vacuole function and morphology in yeast. Mol. Biol. Cell *6*, 525–539.

Zhang, G., Kazanietz, M.G., Blumberg, P.M., and Hurley, J.H. (1995). Crystal structure of the Cys2 activator-binding domain of protein kinase Cδ in complex with phorbol ester. Cell *81*, 917–924.

**Protein Data Bank ID Code**

The coordinates for the structure reported in this paper have been deposited in the Protein Data Bank under ID code 1vfy.